# APPENDIX A

## FORMULATIONS OF DEBRIS ENTRAINMENT PROCESSES

Proceedings of the ANS/ENS International Topical Meeting on
Probability, Reliability and Safety Assessment

Pittsburgh, Pennsylvania
(April, 1989)

# AN EVALUATION OF FISSION PRODUCT RELEASE RATES DURING DEBRIS DISPERSAL

ROBERT E. HENRY
Fauske & Associates, Inc.
16W070 West 83rd Street
Burr Ridge, Illinois 60521
(312) 323-8750

## ABSTRACT

Failure of a reactor pressure vessel under severe accident conditions could result in debris dispersal into the containment if the vessel were at an elevated pressure. This process could influence both containment loading and fission product release from the core debris. Recent modeling approaches have focused on the potential for debris entrainment by high velocity gases resulting from the primary system blowdown. This paper considers both the potential for entrainment, which also results in deceleration of the gas flow as the entrained debris is accelerated, and the simultaneous potential for displacing debris from the reactor cavity without fine scale particulation. If substantial amounts of the debris would be expelled from the cavity region as a relatively continuous mass, limited amounts would be dispersed into the containment atmosphere, and the interfacial area available for heating of the containment atmosphere and for release of fission products from the melt would be minimal. The resulting model is compared with the recent direct containment heating experiments, including those incorporating fission product simulants.

## INTRODUCTION

The spectrum of severe accidents involves conditions wherein water is depleted from the reactor core for tens of minutes, thereby causing the core materials to overheat, oxidize, melt, and slump into the lower head of the reactor vessel. At this point, core debris could fail the reactor vessel through either thermal attack of instrument penetrations in the reactor vessel wall, or through attack of the vessel wall itself. If the vessel wall were penetrated, debris would be discharged into the reactor cavity, followed by blowdown of the primary system gaseous inventory. If the blowdown is sufficient to cause entrainment of the accumulated debris within the reactor cavity, this material could be dispersed into the lower containment compartment. Finely particulated debris from the entrainment process, could be distributed into the containment atmosphere, potentially resulting in a rapid heating and pressurization. Debris dispersal was first addressed in the Zion[1] and Indian Point[2] Probabilistic Safety studies and has been further considered in the Industry Degraded Core Rulemaking (IDCOR and NRC programs[3,4] and in recent probabilistic risk assessments such as Millstone-3[5] and Seabrook.[6] It has also been the subject of several experimental studies using both simulant fluids and prototypic materials.[7,11] A major question for application to reactor systems is whether all the debris would be finely particulated, or would it be displaced from the reactor cavity as a comparatively continuous mass with limited particulation?

Particulation would also increase the fission product release rate from the debris. This would be accelerated due to the area amplification and could result in a significant addition of nonvolatile fission products to the containment atmosphere at the time of reactor vessel failure.

## MODELING APPROACH

Consider the condition shown in Figure 1, i.e., the RPV at a pressure $P_v$ with a failure site area $A_v$ in the lower vessel head. For elevated primary system pressures the gas flow through the breach would be choked. Gases undergoing rapid depressurization expand isentropically unless sufficient energy is transferred to the gas. Generally, this energy transfer is a comparatively slow process. However, in the situation being modeled the expanding gases would receive heat from both deposited and entrained high temperature core debris. This additional energy transfer could occur within the reactor vessel during the expulsion process as well as in the reactor cavity/instrument tunnel. As an approximation to this process, one can assume that the gas expands isothermally, in which case the gas would receive sufficient energy to remain at a constant temperature. Under this condition, the gas mass flow rate is given by

$$\dot{m}_g = P_v A_v \left(\frac{M}{RT}\right)^{0.5} = 0.6\, P_v A_v \left(\frac{M}{RT}\right)^{0.5} \qquad (1)$$

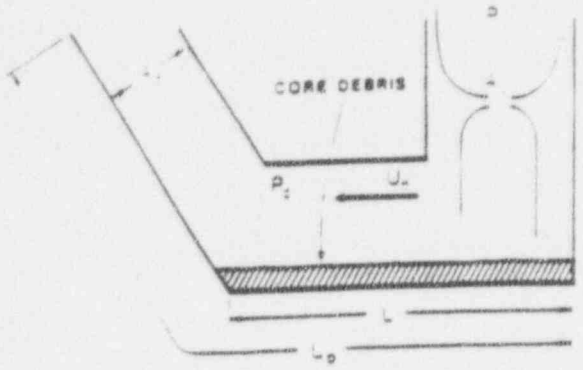


FIGURE 1 SCHEMATIC OF THE MAJOR VARIABLES IN THE MODEL

In a choked isothermal expansion, the ratio of the throat pressure ($P_c$) and the vessel pressure is approximately 0.6.

Given a sufficient gas velocity, entrainment would occur as long as the molten debris resides in the cavity. This minimum entrainment velocity is given by Kutateladze[12]

$$U_g = \frac{3.7\left[g\sigma\left(\rho_D - \rho_g\right)\right]^{0.25}}{\left(\rho_g\right)^{0.5}} \tag{2}$$

As an example, let $\rho_D$ = 7000 kg/m³, $\sigma$ = 1 N/m and $\rho_g$ = 3 kg/m³. For these conditions the entrainment velocity would be about 35 m/sec, which is the minimum gas velocity for entrainment. As illustrated in Figure 2, movement (displacement) of the debris would also be anticipated due to the imposed pressure differential ($P_o - P_c$) created by stagnation of the gas flow discharged from the primary system. The acceleration of debris along the reactor cavity and instrument tunnel (neglecting friction) wall can be represented by

$$a = \frac{F}{m} = \frac{\left(P_o - P_c\right) b\delta}{\rho_D\, b\delta\, L} = \frac{P_o - P_c}{\rho_D\, L} \tag{3}$$

Assuming the acceleration to remain constant, the time required for the core material to traverse the length of the flow path ($L_p$) is

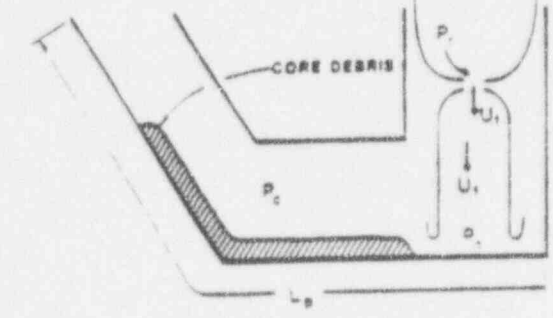


FIGURE 2 SCHEMATIC REPRESENTATION OF DEBRIS DISPLACEMENT

$$t = \left(\frac{2L_p}{a}\right)^{0.5} = \left(\frac{2L_p\,\rho_D}{P_o - P_c}\right)^{0.5} \tag{4}$$

While wall friction is neglected, this is compensated by the assumption that the debris has a long characteristic length (L) which is assumed to remain constant. In actuality, the molten debris would deform into "roll-up waves" which would shorten the effective debris length.

The stagnation pressure imposed by the gas stream on the molten debris can be evaluated by considering the unbounded expansion shown in Figure 2. Given a choked flow condition at the RPV failure location, the one-dimensional momentum equation relating the gas flow rate and the pressure difference between the throat and the point where the expansion is complete is given by:

$$\left(P_t - P_c\right) A_v = \dot{m}_g \left(U_1 - U_t\right) \tag{5}$$

Generally, $P_t \gg P_c$; hence, this can be approximated by

$$U_1 = \frac{P_t\, A_v}{\dot{m}_g} + U_t \tag{6}$$

Furthermore, assuming an isothermal process as represented in Equation (1), this can be reduced to:

$$U_1 = \left(\frac{RT}{M_w}\right)^{0.5} + U_t = 2U_t \tag{7}$$

where the first term in Equation (7) is the flow velocity (choked) at the throat for isothermal expansion. Stagnation of this high velocity gas stream would cause a pressure difference to support flow along the lower surface of the reactor cavity/instrument tunnel configuration. Pressurization due to the stagnation can be evaluated by integration of the compressible Bernoulli equation, again assuming the path to be isothermal, i.e.,

$$\int_{P_c}^{P_o} \frac{dP}{\rho_g} = \int_{U_1}^{0} d\left(\frac{U^2}{2}\right) \tag{8}$$

This yields a prediction for the pressure ratio (stagnation pressure to the cavity pressure):

$$\frac{P_o}{P_c} = \exp\left[\frac{\rho_t}{P_c}\frac{U_1^2}{2}\right] = \exp\left[\frac{U_1^2\, M_w}{2\, RT}\right] \tag{9}$$

Since

$$U_1 = 2U_c = 2\left(\frac{RT}{M_w}\right)^{0.5} \tag{10}$$

the above equation reduces to

$$P_o = 7.4\, P_c \tag{11}$$

This is the pressure which is imposed on the debris and should be used in Equation (3). Hence

$$a = \frac{P_2 - P_1}{\rho_D L} = \frac{0.4\,P_c}{\rho_D L} \qquad (12)$$

As a result, the time for available entrainment, Equation (4) becomes

$$t = \left(\frac{2\,L_p\,L\,\rho_D}{0.4\,P_c}\right)^{0.5} \qquad (13)$$

This development shows that the debris displacement along the channel can be related to the reactor cavity pressure. Therefore, if the cavity pressure is estimated, the time available for entrainment before the debris is displaced out of the reactor cavity and instrument tunnel can be evaluated.

The rate of entrainment between a dense two-phase mixture and the surrounding gas has been addressed by Epstein and Fauske[13] utilizing an entrainment rate relationship developed by Ricou and Spalding.[14] In this approach, the entrainment rate per unit surface area of the debris can be related to the gas velocity by

$$\frac{\dot{m}_e}{A_s} = E_o\left(\frac{\rho_g}{\rho_D}\right)^{0.5} U_c\,\rho_g \qquad (14)$$

Equation (14) can be related to the gas flow rate as

$$\dot{m}_D = 0.1\left(\frac{\rho_g}{\rho_D}\right)^{0.5}\frac{A_s}{A_c}\,\dot{m}_g \qquad (15)$$

By using the minimum cross-sectional flow area, the model evaluates the minimum sizes which could be developed by hydrodynamic fragmentation. Also, since the minimum area usually occurs at the exit of the instrument tunnel, the model accounts for the potential to entrain debris on the reactor cavity floor, deposit the entrained material on the inclined instrument tunnel wall (due to curvature effects), and reentrainment of the molten material by the gas stream. This approach may overstate the potential for debris particulation. As such, this will provide a conservative estimate of the containment load potential. As the debris is entrained, the acceleration of the dense material toward the gas velocity will also cause the gas velocity to decrease. Considering the momentum of the flowing stream to be conserved, the increased momentum of the entrained debris is obtained at the expense of the gas momentum. Assuming that the gas behaves reversibly after the unbounded expansion when it leaves the reactor vessel, conservation of momentum between the gas and debris can be written as

$$\dot{m}_g\,U_c = \left(\dot{m}_g + \dot{m}_D\right)U \qquad (16)$$

(The speed of the entrained debris is assumed to equilibrate with the gas velocity.) The velocity $U_c$ is equal to twice the throat velocity as developed in Equations (1), (6), and (7). Further assuming that the entrained debris does not occupy a substantial fraction of the cross-sectional flow area, Equation (16) can be written as

$$\frac{\dot{m}}{A_c P_c} = \frac{\dot{m}}{1 + 0.1\,\frac{A_s}{A_c}\left(\frac{\rho_g}{\rho_D}\right)^{0.5}}\left(\frac{\dot{m}}{0.6\,A_v P_v}\right) \qquad (17)$$

In general $0.1\,A_s/A_c(\rho_g/\rho_D)^{0.5} \gg 1$ so Equation (17) this can be further approximated by

$$P_c = 0.03\,\frac{A_s}{A_c^2}\left(\frac{\rho_g}{\rho_D}\right)^{0.5} P_v A_v \qquad (18)$$

Due to the approximations involved, this pressure should be limited to the throat pressure for choked flow, or $0.6\,P_v$. When applied to typical test geometries, this results in substantial pressurization because entrainment slows the gas velocity dramatically. This pressurization requires on the order of 100 msec and debris dispersal may be finished before the pressure increases to this level. However, this quasi-steady value provides some measure of the cavity pressurization which influences both the gas jet dynamics as it exits the vessel and the potential for moving debris along the cavity floor.

The gas density, which is a function of the cavity pressure, appears on the right-hand side of the above equation. However, since the value on the right-hand side only varies as the square root of the cavity pressure, it will be assumed that this can be adequately represented by an average value of twice the pressure in the reactor cavity immediately prior to ejection of the core debris. With this expression, the value of the reactor cavity pressure can then be substituted into the expression for the material ejection time from the reactor cavity configuration, Equation (13), to yield

$$t = \left(\frac{10.4\,L_p\,L\,A_s^2}{P_v\,A_s\,A_v}\right)^{0.5}\left(\rho_D\,\rho_g\right)^{0.25} \qquad (19)$$

Multiplying the entrainment rate given in Equation (15) by this interval results in an expression for the total mass entrained by the gas stream before the remainder of the debris is "pushed" out of the reactor cavity as a comparatively coherent liquid mass as

$$m_D = 0.19\,A_v\left[P_v L_p - \rho_D\left(\frac{A_s}{A_v}\right)\left(\frac{M_w}{RT}\right)\left(\frac{\rho_g}{\rho_D}\right)^{0.5}\right]^{0.5} \qquad (20)$$

This is the mass which could interact with the gas atmosphere to rapidly exchange heat and pressurize the containment building, i.e., direct containment heating. Such predictions can be compared with the various direct containment heating experiments.

Consider an example with system properties like those used previously with the additional features of a Zion-like reactor cavity as shown in Figure 1, i.e., a debris characteristic length of $L = 12$ m, a path length of $L_p = 21$ m, and a horizontal surface area of 50 m$^2$. For these conditions the extent of debris which could be entrained by the gas is about 23,400 kg. It should be noted that this analysis only

considers the reactor cavity and instrument tunnel. No consideration is given in these calculations for separation of the debris from the gas stream by structures in the lower containment compartment.

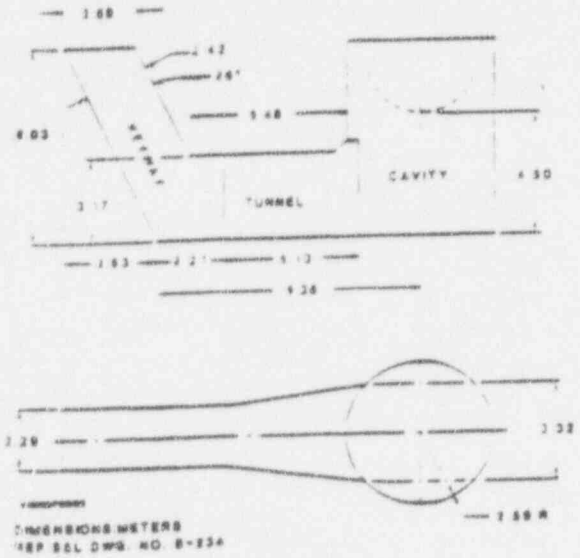


FIGURE 3 ZION-LIKE REACTOR CAVITY AND INSTRUMENT TUNNEL DIMENSIONS

The potential for breaking up molten globules once they are entrained can be related to a critical Weber number (We).

$$We = \frac{\rho U_c^2 d}{\sigma} \qquad (21)$$

For this order of magnitude assessment, it may be assumed that the entrainment occurs immediately as the gas is released from the reactor vessel such that the initial gas velocity in the cavity is the most appropriate value. Using Equation (1) and assuming the gas in the cavity behaves as an ideal gas, this velocity is given by

$$U_c = \frac{0.6\, P_v}{P_{co}} \left(\frac{A_v}{A_c}\right) \left(\frac{\gamma RT}{M_v}\right)^{0.5} \qquad (22)$$

Using the values considered in the previous examples, the initial gas velocity would be about 100 m/sec. An initial cavity pressure of 0.3 MPa is assumed. The particle size, from Equation (21), associated with this velocity is about 110 μm. The maximum velocity which could be developed in the cavity would be the velocity of sound, Hence, $U_c$ should be limited to $(RT/M_v)^{0.5}$. If the sonic velocity at the initial cavity conditions is not sufficient to vent the incoming gas flow, the reactor cavity pressure would increase over its initial pressure to a value sufficient to allow the cavity exit flow to equal the flow from the vessel. For the assumed isothermal expansion, this would occur when

$$P_c = P_v \left(\frac{A_v}{A_c}\right) \qquad (23)$$

At this pressure, the gas density in the reactor cavity and instrument tunnel would be

$$\rho_{gs} = \frac{P_v M_v}{RT} \left(\frac{A_v}{A_c}\right) \qquad (24)$$

Using this density in the Weber number relationship, Equation (21), with the velocity of sound, the stable particulate size can be expressed as

$$d = \frac{We\, \sigma}{P_v \left(\frac{A_v}{A_c}\right)} \qquad (25)$$

The extent of direct heating represented by the mass of debris calculated to be finely distributed can be evaluated by assuming that this debris achieves thermal equilibrium with the gas in the simulated containment volume. Under such conditions, the final temperature ($T_f$) achieved by the debris and gas is given by

$$T_f = \frac{m_a c_{p_a} T_a + m_g c_v T_i + Q_D}{\left(m_g c_v + m_a c_{p_a}\right)} \qquad (26)$$

Assuming perfect gas behavior, the final pressure achieved by the direct heat exchange from the debris to the gas phase can be estimated by

$$P_f = P_i \frac{T_f}{T_i} \qquad (27)$$

This relationship ignores the gas added to the simulated containment as a result of the blowdown process, the oxygen removed from the atmosphere by oxidation, energy transfer from the remainder of the debris, and also energy liberated by further debris oxidation. However, Equation (27) does provide a convenient check on the model with respect to its first order evaluation of peak pressures as a result of the dispersal process. In particular, the relationship developed for the mass dispersed is substantially less than the total mass injected in many experiments and therefore provides a convenient check on the capability of this model to represent the experiments performed to date.

For actual containment configurations of a more complex nature than that illustrated in Figure 1, the above model overestimates the debris entrainment since the shape of the reactor cavity has not been addressed. One would anticipate that the action of flowing through directional changes would cause entrained debris to re-deposit on the channel walls. This process has however not been included in this model. Hence, the resulting calculation for the reactor core should be expected to somewhat overstate the mass of material which could be finely particulated. Thus, the fission product release resulting from such entrainment would be overestimated by the model.

Fission product release involves diffusion of the various materials to the melt surface and convective removal of those materials from the surface. In this analysis, it is assumed that

the release is limited by diffusion through the molten material such that the molar flux of species i is given by

$$\frac{\dot{N}_i}{A} = -D_i \left.\frac{dc_i}{dr}\right|_{r=R} \tag{28}$$

For diffusion in a static droplet, the release can be related to an effective boundary layer of 1/3 the radius. Consequently, Equation (28) can be approximated by

$$\frac{\dot{N}_i}{4\pi R^2} = -D_i \frac{9\,N_i}{4\pi R^3 \cdot R} \tag{29}$$

which reduces to

$$\dot{N}_i = -\frac{9\,D_i\,N_i}{R^2} \tag{30}$$

or

$$\ln\frac{N}{N_o} = -\frac{9\,D_i\,t}{R^2} \tag{31}$$

The time during which debris may exist in the entrained state can be represented by the time of flight. This period can be estimated as the sum of the debris removal time from the cavity and the transit time through the region above the cavity (such as the lower compartment in a reactor configuration) which will be represented as $L_o/U_c$. The parameter $L_o$ is the effective height of the compartment. This results in an expression for the dissolved species remaining in the melt as

$$\ln\left(\frac{N}{N_o}\right) = \frac{9\,D_i}{R^2}\left\{\left[\frac{10.4\,L_o\,L\,A_c}{P_v\,A_s}\right]^{0.5} \cdot \left(\rho_D\,\rho_g\right)^{0.25} \cdot \frac{L_o}{U_c}\right\} \tag{32}$$

If the diffusion coefficient is specified, the fractional releases, as dictated by diffusion to the surface, can be evaluated.

## COMPARISON WITH EXPERIMENTS

### SURTSEY Tests

DCH-1. The DCH-1 test used 20 kg of molten iron thermite in the melt generator with approximately 11.6 kg being dispersed out of the reactor cavity into the large test vessel. The melt was doped with lanthanum oxide, barium molybdate, niobium pentoxide, and nickel to simulate dissolved fission products. Table 1 (from Reference 7) delineates the experimental initial conditions and the masses of fission product simulants. The test configuration, which includes a chute installed on the end of the instrument tunnel, is shown in Figure 4. The important dimensions for model application were taken from Reference 7.

TABLE 1 DCH-1 INITIAL CONDITIONS

| | |
|---|---|
| Melt Mass | 20.0 kg |
| Thermite Composition | Iron Oxide[a] ($Fe_3O_4$) 76.2 Mass % Plus Aluminum[b] (Al) 23.8 Mass % |
| Melt Composition (Fully Reacted) | Iron (Fe) 55.2 Mass % Plus Alumina ($Al_2O_3$) 44.8 Mass % |
| Dopants | Lanthanum Oxide ($La_2O_3$) - 118 g, Barium Molybdate ($BaMoO_4$) - 313 g, Niobium Pentoxide ($Nb_2O_5$) - 143 g, Nickel (Ni) - 100 g |
| Ambient Temperature | 26°C |
| Ambient Pressure | 0.08 MPa (12.0 psia) |
| Driving Gas | Dry Bottled Nitrogen ($N_2$) |
| Melt Generator Gas Volume | 0.109 m³ (41.1 cm Diameter by 156.7 cm Long) |
| Initial Gas Pressure | 1.86 MPa (270 psig) |
| Fusible Plug Diameter | 4.8 cm |

a. Chemalloy MS-30 (100% minus 30 mesh).
b. ALCOA Atomized Powder (flake form).

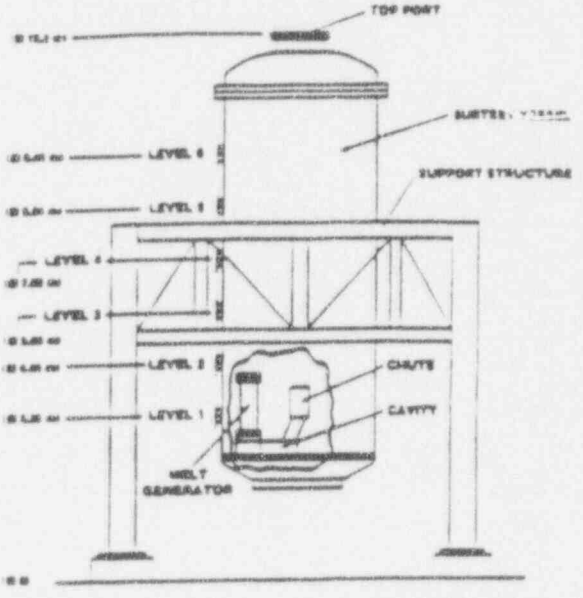


FIGURE 4 SCHEMATIC OF THE DCH-1 APPARATUS IN THE SURTSEY DIRECT HEATING TEST FACILITY

As a result of heating during the thermite reaction, the crucible pressure increased to a maximum of about 2.4 MPa, which would correspond to an average gas temperature of 386K. With the geometrical parameters given in Table 2, the debris particulation can be evaluated through the Weber number criteria. As shown in Table 2, this results in a predicted size which is somewhat smaller than the measured mass mean. This small predicted debris size may be due to the use of the minimum cross-sectional area in the model, which usually occurs at the exit of the instrument tunnel. If a value typical of the horizontal segment of the tunnel (where the entrainment initially occurs) had been used, a larger debris size would have been predicted.

Table 2 also lists the predicted peak pressure and temperature in the SURTSEY vessel along with the measured values. As shown, the model predicts that the total mass used in the melt generation could be dispersed as fine scale debris. Reference 7 lists the locations where debris was deposited and a significant fraction (~ 0.5) was found to be frozen in the melt generator and the reactor cavity. This potential for freezing debris on the reactor cavity and instrument tunnel walls was not included in the thermal-hydraulic model. As a result, the driving potential is sufficient to disperse essentially all of the melt in the generator. Thus, there was sufficient potential to particulate and disperse the available molten materials. This condition of having the potential to entrain and disperse more material than is available in a molten state is only observed for the DCH-1 test, in which only 20 kg of thermite was used. For all subsequent experiments (DCH-2, -3 and -4), 80 kg of thermite was used, and the melt mass exceeds the potential for entrainment and dispersal.

As applied to the DCH-1 test, the model results is a prediction consistent with the observation, i.e., all the available melt would be dispersed. Since the rapidly frozen material was not dispersed, the maximum temperature and pressure calculations are compared to measure conditions by using the measured mass dispersed from the cavity. By using the measured mass, the applicability of the modeling approach to represent the energy transferred to the gas space can be tested. As observed by the comparisons shown in Table 2 for peak pressure and temperature, the model is consistent with the DCH-1 test results.

For the maximum pressure and temperature predictions, the reaction heat was assumed to be negligible. Measurements of oxygen depletion from the atmosphere following the DCH-1 test were not sufficiently accurate to determine the extent of reaction. However, the DCH-4 test, was performed in an inert atmosphere, and the pressure rise and peak pressure were not greatly

TABLE 2 MODEL COMPARISONS FOR DCH TEST

| Test Parameters/ Predictions/ Measurements | DCH-1 | DCH-2 | DCH-3 | DCH-4 |
|---|---|---|---|---|
| 1. Geometrical Parameters and Vessel Pressure | | | | |
| $A_c$ (m²) | 0.002 | 0.002 | 0.002 | 0.002 |
| $A_v$ (m²) | 0.5 | 0.5 | 0.5 | 0.5 |
| $L_1$ (m) | 2.8 | 2.3 | 2.8 | 2.8 |
| $L_2$ (m) | 1.45 | 1.45 | 1.45 | 1.45 |
| $L_3$ (m) | 0.06 | 0.06 | 0.06 | 0.06 |
| $P_v$ (MPa) | 2.5 | 6.8 | 6.8 | 6.8 |
| 2. Debris Size | | | | |
| Predicted (μm) | 260 | 65 | 48 | 38 |
| Measured Mass Mean (μm) | 550 | Not Available | Not Available | Not Available |
| 3. Mass Dispersed as Fine Particulate | | | | |
| Predicted (kg) | 20 | 27 | 31 | 33 |
| Measured (kg) | 11.6 | 33 (Mass Deposited on the Lower Head) | 18.4 (Mass Deposited on the Lower Head) | 38 (Mass Deposited on the Lower Head) |
| 4. Peak Temperature | | | | |
| Predicted (K) | 661 (Using Measured Mass Dispersed) | 1032 | 1104 | 1138 |
| Measured (K) | 581 | 1150 | 1193 | 1193 |
| 5. Peak Pressure | | | | |
| Predicted (MPa) | 0.18 (Using Measured Mass Dispersed) | 0.30 | 0.32 | 0.33 |
| Measured (MPa) | 0.18 | 0.33 | 0.28 | 0.27 |

different from those in the DCH-3 test which had an air atmosphere in the vessel. Consequently, the oxidation must occur over an interval in which the vessel heat sinks are also very important. Therefore, in all of the adiabatic representations of peak pressure and temperature, the reaction heat has been neglected.

DCH-2. This experiment provides a more meaningful test of the model since it used a larger melt inventory (80 kg) and higher nitrogen driving pressure (4.03 MPa). The reactor cavity/instrument tunnel configuration was similar to DCH-1 but did not use a chute at the end of the instrument tunnel.

The driving pressure increased to a maximum of 6.8 MPa during the reaction which corresponds to an increase in the average gas temperature to ~91K. Using these values with the geometrical parameters listed in Table 2 results in a predicted mass of finely particulated debris of 27 kg at the diameter of 65 μm - the remainder of the debris being dispersed without fine particulation.

The DCH-2 debris characterization is greatly different from that in DCH-1. Large quantities of debris were found frozen on the vertical walls and the upper head of the SURTSEY vessel. Such observations are consistant with the modeling approach in that 27 kg is predicted to be fine particulated, entrained and dispersed while the remainder of the material would be dispersed as a relatively coherent mass. Molten debris dispersed as a comparatively continuous mass could impact the vessel vertical wall, freeze as a crust, the thickness of which would be dictated by the heat transfer into the steel, and the remainder could continue to flow upward to the head. Finely particulated material would rapidly exchange heat with the vessel atmosphere, freeze and fall to the lower head. Thus, mass recovered from the lower head (33 kg) can be compared to, and is in agreement with, the predicted value of 27 kg.

The predicted peak pressures and temperatures are in agreement with the observed values but somewhat understate the results. This may be due to either limited oxidation during the expulsion process or some heat transfer to the atmosphere from the fraction of debris which was not fine particulated but nonetheless was expelled from the instrument tunnel, impinged on the SURTSEY vessel wall, and froze. Neither of these are currently included in the model. The DCH-4 test with an inert atmosphere, which is discussed later, shows the same general behavior as DCH-2. This indicates oxidation of the fragmented material in these tests is not a first-order process in terms of heating the gas atmosphere. Hence, it is reasonable that the model ignore oxidation.

DCH-3. This test has not been fully reported and the extent of experimental observations is limited.[9] Conditions used for the model benchmark are an initial melt inventory of 80 kg and a configuration like DCH-1 with a chute added to the exit of the instrument tunnel. Table 2 lists the geometrical parameters and the predicted values for debris size, mass dispersed, peak temperature, and peak pressure. As shown, the model predictions are in agreement with the observed peak pressure and temperature. Since the extent of particulated debris is not presently available, the predicted value is compared with that accumulated on the lower head of the SURTSEY vessel as it was with the DCH-2 test. As discussed previously, this represents the finely divided material which froze during transit through the containment atmosphere while also being decelerated quickly after being discharged from the instrument tunnel. Both of these would tend to keep this material in the vessel atmosphere such that it would eventually settle on horizontal surfaces, i.e., the vessel lower head. The comparison shows the model somewhat overpredicts the experimental result.

DCH-4. This test was virtually identical to DCH-3 (including 80 kg of thermite and use of a chute) except the SURTSEY vessel atmosphere was inerted. The model does not use rapid oxidation to assess the peak pressure. Hence, the predictions for this test are very close to those of DCH-3. Table 2 lists the parameters for the DCH-4 comparison. The predicted and measured values of the vessel pressure and temperature are in agreement with the test results. Also, the mass of debris removed from the vessel lower head agrees with the material mass predicted to be finely particulated. Comparison of these results with those of DCH-3 may indicate the level of resolution for the data. In particular, the measured peak temperatures are in agreement, yet the final disposition of debris on the lower head differs by 40%. Hence, this is likely the resolution of the experimental information at this time, subject to more detailed reporting of the experimental results of tests DCH-3 and DCH-4.

In summary, these comparisons with the four DCH tests run in the SURTSEY facility show the proposed model to be consistent with the test observations. These comparisons include the mass which could be finely particulated, the peak vessel pressure, and the peak vessel temperature.

Comparison With Fission Product Release Data

The DCH-1 test used fission product simulants to represent the dissolved low volatile species in the debris. If the time for fission product release is the time of flight, the appropriate time for the DCH-1 test would be the time the material is resident in the cavity (~ 0.04 seconds) plus the time of flight between the cavity mouth and the upper head (~ 0.07 seconds). The results in a flight time of about 0.1 seconds. If the $\alpha_g$ diffusivities are considered to be about $10^{-8}$ $m^2$/sec, about 10% of the fission product would be released from the fine particulated material. Since the finely fragmented and dispersed mass was about 50% of the debris in DCH-1, this corresponds to approximately 5% of the inventory. Table 3 lists the measured release fractions for the various

materials in this test. The estimated release value characteristic of the overall inventory of approximately 5% is in general agreement with these data. Such variations are well within the uncertainty bounds of the limited data base for diffusivities in the melt.

TABLE 3 MEASURED ELEMENTAL AEROSOL RELEASE FRACTIONS IN DCH-1

| Element | Mass in Relocated Debris[a] (g) | Mass in Aerosol[b] (g) | Release Fraction[c] (%) |
|---|---|---|---|
| Fe | 5610 | 353 | 6.3 |
| Al | 2430 | 44 | 1.81 |
| Mo | 51.5 | 9.8 | 19.0 |
| Ni | 51.0 | 4.8 | 9.4 |
| Nb | 51.0 | 0.98 | 1.92 |
| Ba | 73.7 | 1.11 | 1.51 |
| La | 51.3 | 0.35 | 0.68 |

a. Uncertainty in relocated mass = ± 10%.
b. Uncertainty in aerosol mass = ± 53%.
c. Resulting uncertainty in release fraction = ± 54%.

## SUMMARY OF RESULTS AND CONCLUSIONS

The issue of fission product release during the primary system blowdown following melthrough of the reactor vessel lower head has been addressed by developing a model for the extent of fine scale debris particulation and the resultant diffusion of low volatility fission products in the melt fragments. This model also relates to the issue of direct containment heating. The model has been benchmarked with the results of the DCH tests performed at SNL. Such comparisons have demonstrated that the model predictions agree with the observed peak pressures and temperatures, especially the tests using a larger melt mass. The current model addresses only the reactor cavity and instrument tunnel configuration, and ignores the lower compartment structures. Consequently, the model represents a conservative assessment of the potential influence of direct containment heating on current containment configurations.

The model also predicts the scale of debris particulation and the diffusion of fission products to the surface of this finely dividad debris. This model was compared with the results of the SNL DCH-1 test. A comparison of the model predictions to the data show agreement with the test results with the major uncertainty being the diffusivity of the fission products (or their simulants) in the finely particulated debris.

## ACKNOWLEDGEMENT

Prepared for EG&G Idaho, Inc. Under Subcontract No. C85-100740 and the U.S. Department of Energy Under Contract No. DE-AC07-76ID01570.

## REFERENCES

1. "Zion Probabilistic Safety Study" Commonwealth Edison Company September, 1981).

2. "Indian Point Probabilistic Safety Study" Prepared for Power Authority of the State of New York and Consolidated Edison Company of New York, Inc., (March, 1982).

3. "Technical Support for Issue Resolution", IDCOR Technical Report 85.2, Atomic Industrial Forum, (July, 1985).

4. U.S. NUCLEAR REGULATORY COMMISSION (USNRC), "Reactor Risk Reference Document", Draft, NUREG-1150, (February, 1987).

5. NORTHEAST UTILITIES, "Millstone-3 Probabilistic Safety Study", (August, 1983).

6. PICKARD, LOWE AND GARRICK, INC., "Seabrook Station Probabilistic Safety Assessment" Prepared for Public Service Company of New Hampshire and Yankee Atomic Electric Company, PLG-0300, (December, 1983).

7. W.W. TARBELL, ET AL., "Results From the DCH-1 Experiment", Sandia National Laboratory Report, NUREG/CR-4871, (June, 1987).

8. W.W. TARBELL, ET AL., "DCH-2: Results From the Second Experiment Performed in the SURTSEY Direct Heating Test Facility", Sandia National Laboratory Report, NUREG/CR-4917, (January, 1988).

9. W.W. TARBELL, ET AL., "DCH Experiments and Analyses at Sandia National Laboratories" Presentation to the NUREG-1150 Containment Loads and Molten Core Containment Expert Opinion Meeting, (December 15-18, 1987), Albuquerque, New Mexico.

10. B.W. SPENCER, ET AL., "Corium/Water Dispersal Phenomena in Ex-Vessel Cavity Interactions", Proc. Intl. Mtg. on Light Water Reactor Severe Accident Evaluation, Cambridge, Massachusetts, (August 28 - September 1, 1983), American Nuclear Society Publication, Vol. 2, pp. 15.5-1 through 15.5-7.

11. B.W. SPENCER, ET AL., "Hydrodynamics and Heat Transfer Aspects of Corium-Water Interactions, EPRI NP-5127, Electric Power Research Institute, Palo Alto, California, (March, 1987).

12. S.S. KUTATELADZE, "Elements of the Hydrodynamics of Gas-Liquid Systems", Fluid Mechanics/Soviet Research, 4, 1, (1972), p. 29.

[3] H K. FAUSKE and M. EPSTEIN. "Source Term Considerations in Connection with Chemical Accidents and Vapour Cloud Modeling". Journal of Loss Prevention Process Industry. 1. (April, 1988). pp. 75-83.

[4] F B. RICOU and D B. SPALDING. "Measurements of Entrainment by Axisymmetrical Turbulent Jets". Journal of Fluid Mechanics. 11. (1961). pp. 21-32.

NOMENCLATURE

| | |
|---|---|
| $A$ | surface area of a droplet of radius R |
| $A_c$ | minimum cavity flow area |
| $A_s$ | horizontal surface area of the reactor cavity and instrument tunnel |
| $A_v$ | RPV failure area |
| $b$ | width of the cavity |
| $C_i$ | concentration |
| $c_v$ | gas specific heat at constant volume |
| $c_D$ | debris specific heat |
| $D_i$ | diffusivity (or diffusion coefficient) of fission product i in the melt |
| $E_o$ | entrainment coefficient |
| $g$ | acceleration of gravity |
| $L$ | effective length of the debris |
| $M_w$ | gas molecular weight |
| $m_g$ | mass of gas in the volume |
| $\dot{m}_g$ | gas mass flow rate |
| $P_c$ | pressure in the reactor cavity |
| $P_{co}$ | pressure in the cavity at the start of the blowdown |
| $P_v$ | RPV pressure |
| $Q_R$ | heat of reaction |
| $R$ | universal gas constant |
| $r$ | droplet radius |
| $T$ | absolute temperature |
| $T_1$ | initial temperature of the gas |
| $T_D$ | initial temperature of the debris |
| $U$ | homogeneous mixture velocity of the gas and the entrained debris in the reactor cavity |
| $U_c$ | gas velocity over the molten material |
| $U_r$ | relative velocity |
| $U_v$ | gas velocity after the expansion |
| $\rho$ | density of the two-phase flowing stream |
| $\rho_D$ | debris density |
| $\rho_g$ | gas density |
| $\sigma$ | liquid (debris) to gas surface tension |
| $\delta$ | debris depth |

# APPENDIX B

## Calculations of DCH Temperature and Pressure Rise

An important consequence of vessel failure is an increase in containment pressure. Direct containment heating by core debris expelled at vessel failure may be a significant contributor to the total containment pressure increase. This appendix provides a method for estimating the energy released to the containment atmosphere by the core debris released due to high pressure melt ejection following vessel failure.

Although the level of DCH is determined from the amount of energy that is transferred to the containment atmosphere, there are many factors that can affect the actual amount of energy transfer. Overall, the physicochemical and thermofluid dynamical processes leading to DCH are highly complex. These individual factors and processes can be summarized as follows:

1) The mode of reactor failure which determines

   1.1) reactor vessel pressure at the time of vessel failure,

   1.2) failure size,

   1.3) fraction of core mass that would be ejected into the cavity.

2) The amount, temperature and size of the ejected mass that would be dispersed into the containment atmosphere by the follow-on high velocity steam/gas flow which are affected by

   2.1) quenching of debris by water possibly present in the cavity prior to vessel failure,

2.2) enhanced dispersal of debris by water possibly present in the cavity prior to vessel failure due to vigorous steam generation,

2.3) dispersal process including displacement and entrainment of molten debris.

3) Redirection and subsequent de-entrainment of debris particle due to structural impediment (such as seal table structure).

4) Shortening of particle flight time due to redirection of debris onto floor at the tunnel exit and due to structural barriers in the lower compartment.

5) Deposition of debris on structures.

6) Extent of chemical reactions which include oxidation of metallic constituents with steam and oxygen and hydrogen combustion.

The method to be used to estimate the core debris energy release that could contribute to direct containment heating is based on the assumption that the debris mass successfully entrained into the containment atmosphere equilibrates thermally with the containment atmosphere. The evaluation includes the debris superheat, the debris latent heat, the debris sensible heat, as well as the energy produced by oxidation of corium constituents (Zr, Fe, $UO_2$) and by combustion of hydrogen.

The final atmospheric temperature ($T_e$) is the solution of the following energy balance based on thermal equilibration:

debris super heat latent heat of fusion

$$f_e\, m_D \sum C_{cj}\, w_j\, (T_c - T_{cmj}) + f_e\, m_D \sum H_{fj}\, w_j$$

sensible heat — heat of reaction with steam

$$+ f_e m_D \sum C_{cj} w_j (T_{cmj} - T_f) + f_e m_D \sum_{H_2O} f_j w_j \Delta E_j$$

heat of reaction with oxygen — heat of hydrogen combustion

$$+ f_e m_D \sum_{O_2} f'_j w_j \Delta E'_j + \left( m_H + 2 m_D f_e \sum_{H_2O} \frac{f_j w_j}{M_j} \ell_j \right) \Delta E_H$$

gas and steam sensible heat

$$- (m_s C_{vs} + m_g C_{vg})(T_f - T_g) - m_{sps} C_{vs} (T_{PS} - T_f)$$

$$+ \text{HEAT LOSS (assumed zero)} \qquad \text{(B-1)}$$

where:

$C_{cj}$ = specific heat of corium species j [kJ/kg • K],

$C_{vg}$ = specific heat at constant volume of air [kJ/kg • K],

$C_{vs}$ = specific heat at constant volume of steam [kJ/kg • K],

$\Delta E_j$ = heat of reaction of corium species j with steam [MJ/kg species j],

$\Delta E'_j$ = heat of reaction of corium species j with oxygen [MJ/kg species j],

$\Delta E_H$ = heat of combustion of hydrogen [MJ/kg] (set $\Delta E_H$ to zero if no $H_2$ burn is assumed),

$f_e$ = fraction of corium entrained to containment atmosphere,

= 1 - $\alpha$ ($\alpha$ = de-entrainment fraction due to structural impediment obtained from Equation (2-1)),

$f_j$ = fraction of corium species j reacted with steam,

$f'_j$ = fraction of corium species j reacted with oxygen,

$H_{fj}$ = latent heat of fusion of corium species j [MJ/kg],

$\ell_j$ = molar ratio of hydrogen produced to reactant corium species j consumed during steam oxidation (see Table B-1),

$m_D$ = total debris mass entrained from cavity [kg] (determined by Equation 20 of Appendix A),

$m_{cj}$ = mass of corium species j in the pressure vessel [kg],

$m_g$ = initial mass of air in the containment,

$m_H$ = mass of hydrogen expelled from RPV during high pressure melt ejection,

$m_s$ = total mass of steam in the containment prior to high pressure melt ejection [kg],

$m_{sps}$ = steam mass expelled from RPV at vessel failure [kg],

$= P_{PS}V_{PS}/RT_{PS}$,

$M_j$ = atomic mass of corium species j [kg/kmol],

$P_{PS}$ = primary system pressure at vessel failure [Pa],

$T_c$ = temperature of corium prior to vessel failure [K],

$T_{cmj}$ = melting temperature of corium species j [K],

$T_f$ = final containment air temperature [K],

$T_{PS}$ = primary system temperature at vessel failure [K],

$T_g$ = temperature of air in the containment prior to high pressure melt ejection [K],

R = universal gas constant = 8.314 [kJ/kmol•K],

$V_{PS}$ = primary system volume [$m^3$],

$w_j$ = mass fraction of corium species j.

Subscript

j = refers to corium species such as $ZrO_2$, $UO_2$, Zr and stainless steel (Fe, Ni, Cr).

Summation

$\sum_{H_2O}$ sum over species reacting with steam,

$\sum_{O_2}$ sum over species reacting with oxygen.

Solving Equation (B-1) for $T_f$ yields

$$T_f = \frac{1}{C_{vg} + \gamma C_{vs} + \epsilon \sum C_{cj} w_j} (\epsilon S_1 + \epsilon S_2 + \beta \Delta E_H + C_{vg} T_g + \gamma C_{vs} T_{PS}) \quad (B\text{-}2)$$

where:

$$S_1 = \sum C_{cj} w_j T_c + \sum H_{fj} w_j + \sum_{H_2O} f_j w_j \Delta E_j + \sum_{O_2} f'_j w_j \Delta E'_j$$

$$S_2 = 2 \sum_{H_2O} \frac{f_j w_j}{M_j} \ell_j \Delta E_H$$

$\epsilon$ = entrained mass ratio = $f_e m_D \Big/ \left( m_g + m_s \frac{C_{vs}}{C_{vg}} \right)$,

$\beta$ = primary system hydrogen mass ratio = $m_H \Big/ \left( m_g + m_s \frac{C_{vs}}{C_{vg}} \right)$,

$\gamma$ = primary system steam mass ratio = $m_{sps} \Big/ \left( m_g + m_s \frac{C_{vs}}{C_{vg}} \right)$.

Information necessary for calculating terms in Equation (B-2) is provided in Tables B-1, B-2, and B-3. Note that $S_1$ in Equation (B-2) represents a collection of properties of corium such as heat capacity, heat of fusion, heat and extent of reactions, corium composition, and corium superheat. $S_2$ represents heat of combustion of hydrogen (per unit mass of corium) produced by steam oxidation of metallic contents of debris during high pressure melt ejection. Given large uncertainty in our knowledge of corium properties under postulated severe accident conditions, it is reasonable to view $S_1$ and $S_2$ approximately as a constant for plants of similar design under similar accident conditions. On the other hand, parameters like $\epsilon$, $\beta$ and $\gamma$, which represent dimensionless mass of entrainment, of hydrogen and of steam, can vary from plant to plant. However, if

values of $\epsilon$, $\beta$ and $\gamma$ are made the same for two plants, a calculation of $T_f$ from Equation (B-2) for one plant will also be for another plant. These parameters will be helpful in scaling results from one plant to another plant without having to repeat similar calculations.

The containment final pressure ($P_f$), assuming the applicability of the ideal gas laws, is determined from the knowledge of $T_f$ of Equation (B-2) by

$$P_f = \frac{T_f R}{V_c + V_{ca}} \left[ \underbrace{\frac{m_g}{M_g}}_{\text{containment air}} + \underbrace{\frac{m_s}{M_s}}_{\text{containment steam}} + \underbrace{\frac{m_{sps}}{M_s}}_{\text{blowdown mass}} \right] \qquad \text{(B-3)}$$

where:

$M_g$ = average molecular weight of dry air,

$M_s$ = molecular weight of steam,

$P_f$ = containment final pressure [Pa],

$V_c$ = containment free volume [$m^3$],

$V_{ca}$ = cavity/tunnel volume [$m^3$].

Table B-1
(Adapted from [Pilch, et al., 1986] and [Spencer, et al., 1988]

OXIDATION OF DEBRIS CONSTITUENTS IN AN OXYGEN ENVIRONMENT

| Reaction | Heat of Reaction Per Unit Mass of Reactant [MJ/kg] |
|---|---|
| $Zr + O_2 \text{ ---> } ZrO_2$ | 11.8 |
| $Fe + 1/2\ O_2 \text{ ---> } FeO$ | 4.78 |
| $3UO_2 + O_2 \text{ ---> } U_3O_8$ | 0.483 |

OXIDATION OF DEBRIS CONSTITUENTS IN AN STEAM ENVIRONMENT

| Reaction | Heat of Reaction Per Unit Mass of Reactant [MJ/kg] |
|---|---|
| $Zr + 2H_2O \text{ ---> } ZrO_2 + 2H_2$ | 6.74 |
| $Fe + H_2O \text{ ---> } FeO + H_2$ | 0.43 |
| $3Fe + 4H_2O \text{ ---> } 4H_2 + Fe_3O_4$ | 0.98 |
| $2Cr + 3H_2O \text{ ---> } 3H_2 + Cr_2O_3$ | 4.2 |
| $Ni + H_2O \text{ ---> } NiO + H_2$ | 0.04 |

HYDROGEN COMBUSTION

| Reaction | Heat of Reaction Per Unit Mass of Reactant [MJ/kg] |
|---|---|
| $H_2 + 1/2\ O_2 \text{ ---> } H_2O$ | 121 |

Table B-2

PROPERTIES OF CORE DEBRIS CONSTITUENTS

| Material | Density $\rho$ ($kg/m^3$) | Thermal Conductivity k (W/m K) | Specific Heat Capacity* (J/kg K) | Melting Point (K) | Latent Heat of Fusion (MJ/kg) |
|---|---|---|---|---|---|
| Carbon Steel | 8,000. | 50.0 | 797[1]<br>864[2] | 1,800. | 0.250 |
| Zircaloy | 6,500. | 18.0 | 356 | 2,098. | 0.225 |
| Zircaloy Oxide | 5,600. | 3.0 | 645 | 3,000. | 1.196 |
| Uranium Oxide | 10,100. | 3.3 | 491[1]<br>698[2] | 3,113. | 0.274 |

[1] At temperature of 2501 K.

[2] At temperature of 3001 K.

## Table B-3

**PRIMARY SYSTEM AND CORE DEBRIS CONDITIONS FOR DCH ASSESSMENT (In accordance with NUREG-1150, Vol. 3, Appendix J.5)**

| | |
|---|---|
| Reactor Coolant System Pressure ($P_{PS}$) | 600-2400 psig |
| Reactor Coolant System Temperature ($T_{PS}$) | Corresponding Saturation Temperature |
| Melt Temperature ($T_c$) | 1800-2500 K |
| Fraction of Core Melted and Ejected | 20-80% |
| Unoxidized Metal Content | 20-70% |
| Hydrogen Generated in Core ($m_H$) | Proportional to Fraction of Oxidized Metal (30-80%) |
| Completeness of Chemical Reactions* | 50-95% |

*Large uncertainty remains in estimating the extent of oxidation reactions with steam and oxygen which depend strongly on the debris temperature. As ballpark figures, the analyses of CWTI-DCH experiments suggest the following

$$f_j = \begin{cases} 0.75 & \text{for fully wet cavity regardless of water in the lower compartment} \\ 0.5 & \text{for dry cavity and wet lower compartment} \end{cases}$$

and

$$f'_j = \begin{cases} 0 & \text{for fully wet cavity with Zion-type impediment at tunnel exit} \\ 0.05 & \text{for fully wet cavity without impediment at tunnel exit} \\ 0.31 & \text{for dry cavity with Zion-type impediment at tunnel exit} \\ 0.67 & \text{for dry cavity without impediment at tunnel exit} \end{cases}$$

These values represent the conditions for the small scale ($3\frac{1}{3}$%) mockup, and should be considered as the lower bound for a reactor scale. The effects of presence of water are made clear in the values of $f_j$ and $f'_j$.

# APPENDIX C

## Hydrogen Combustion Limits

Numerous experiments have been performed to establish the combustion limits of hydrogen as a function of hydrogen concentration and inert gases. One such study [Benedick, 1984] provided a demonstration of the inerted capabilities of carbon dioxide. The results for these experiments peformed in the VGES test vessel at Sandia are illustrated in Figure C-1, which is taken from Reference [Benedick, 1984]. This also shows the results of other experiments at Lawrence Livermore and Sandia using steam as the inerting material. As shown, the atmosphere becomes inerted at a $CO_2$ concentration of 52%.

A substantial experimental program was performed in the FITS vessel at Sandia to clearly define the combustion boundaries for a hydrogen-air-steam mixture both in quiescent conditions and in a turbulent environment (fans operational). This set of experiments is particularly meaningful to accident management evaluations because (1) steam is the inerting medium, (2) the boundary is clearly defined and (3) the experimental apparatus took great pains to attempt ignition of the mixture. Figure C-2 taken from Reference [Marshall, 1986] illustrates the test results for both the "fans off" and "fans operational" conditions. Those conditions which are represented as "no burn" represent the mixture state in which neither repeated spark initiators nor a glow plug was capable of initiating a burn.

The experimental information was subsequently formulated into a correlation to represent the combustion limits. This is given by

$$\% \text{ Steam} = 100 - \% H_2 - 37.3e^{-0.007\% H_2} - 518e^{-0.488\% H_2} \qquad \text{(C-1)}$$

and is compared to the experimental results in Figure C-2. This result is particularly meaningful to accident management guidance since it demonstrates that containment buildings could be absolutely inerted against hydrogen combustion with a steam concentration of approximately 53%. This

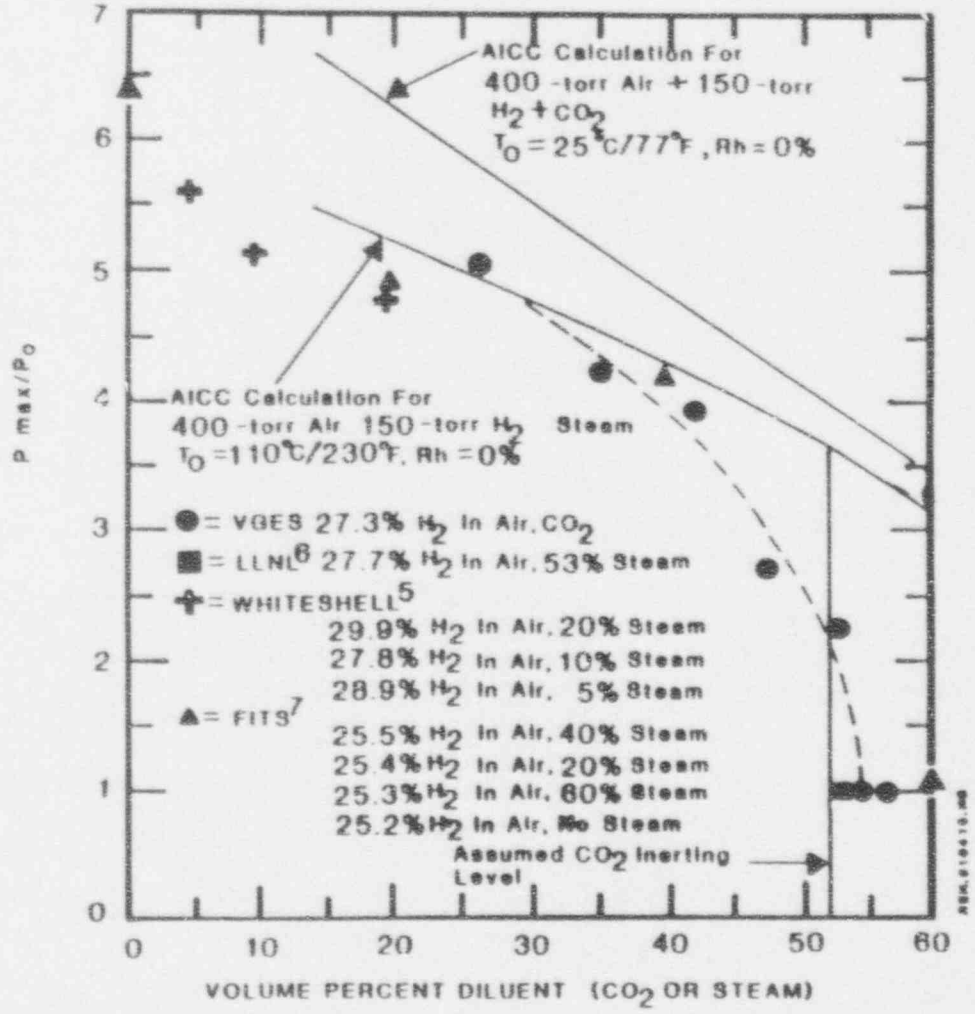


Figure C-1 Normalized peak pressure ($P_{max}/P_o$) for hydrogen:air:diluent mixtures, comparing $CO_2$ and steam (AICC = adiabatic isochoric complete combustion, Rh = relative humidity).

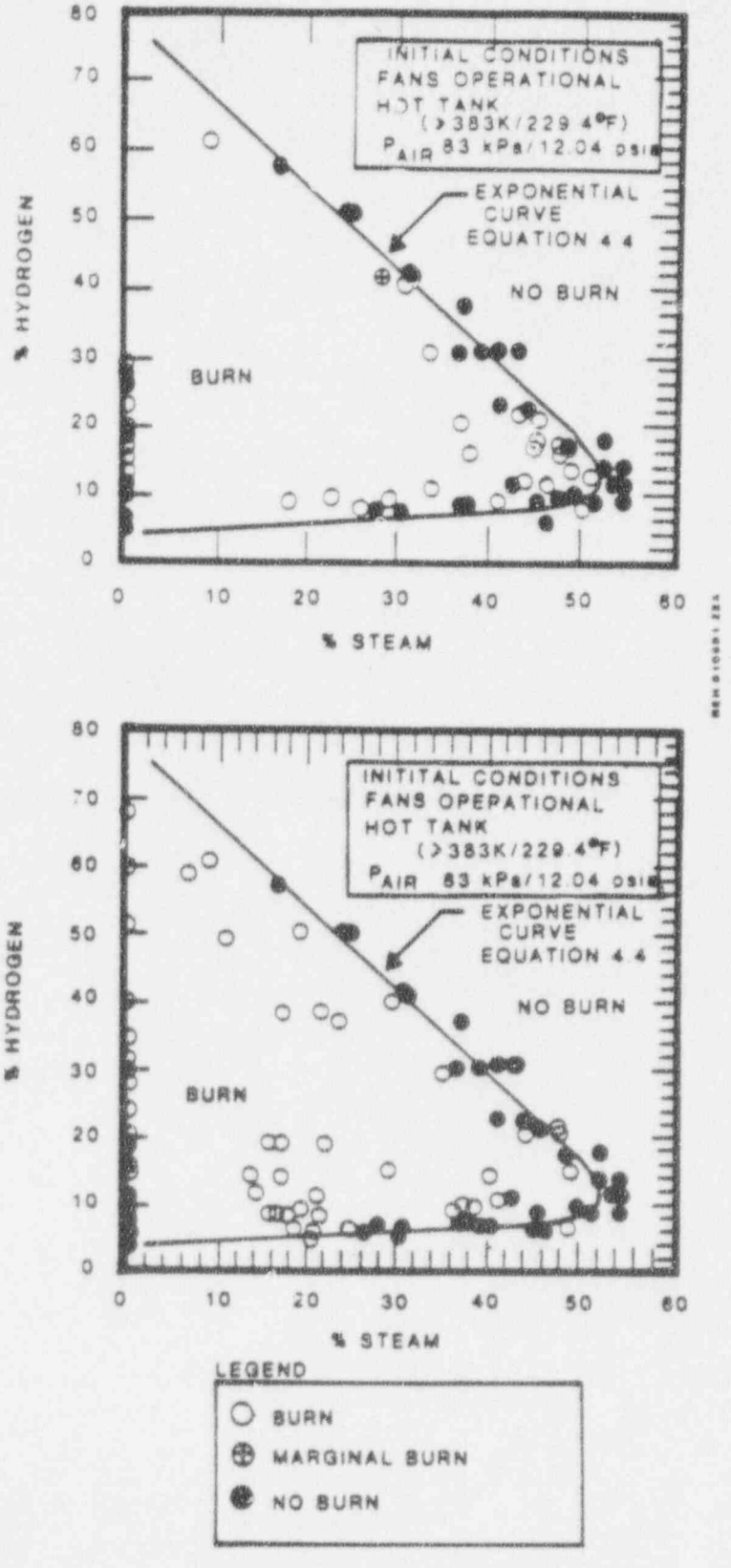


Figure C-2 Experimental data for combustion limits with fans on and off shown with the exponential curve fit.

means that if sufficient steam is released to a non-inerted containment building to produce a steam partial pressure of slightly over one atmosphere, hydrogen combustion would be precluded regardless of how much hydrogen was accumulated in containment. Since steam would be produced as a natural consequence of the accident condition the containment could be completely inerted prior to vessel failure. This should be assessed, where necessary, on a sequence specific basis.

# APPENDIX D

## Scaling of Entrainment and Displacement Rates

For scaled experiments to provide a meaningful representation of the reactor condition, the experiment should exhibit the same relative rates of debris entrainment and displacement, i.e. the ratio of the rates should be the same. As discussed in Appendix A, we can use the Ricou-Spalding correlation to represent the entrainment rate.

$$\dot{m}_e = C_1 A_s \sqrt{\rho_D \rho_g} U_c \qquad \text{(D-1)}$$

where $A_s$ is the cavity floor area available for entrainment. The displacement rate can be viewed as the mass of core debris over the displacement time.

$$\dot{m}_D = m_c / t_D \qquad \text{(D-2)}$$

Assuming a constant acceleration (constant pressure differential), the displacement time is given by,

$$t_D = \sqrt{\frac{2L_p}{a}} = \sqrt{\frac{2\ \rho_D L_p L}{\Delta P}} \qquad \text{(D-3)}$$

where a is the acceleration ($a = \Delta P/(\rho_D L)$) and the terms L and $L_p$ are defined in Figure 2-10.

The pressure differential can be related to the gas dynamic head,

$$\Delta P \approx \frac{\rho_g U_c^2}{2} \qquad \text{(D-4)}$$

such that

$$\dot{m}_D = 0.5\ \delta_b \sqrt{\frac{L_p}{L}} \sqrt{\rho_D \rho_g}\ U_c \qquad \text{(D-5)}$$

Formulating the ratio between the two rate dependent processes yields,

$$\frac{\dot{m}_e}{\dot{m}_D} = \frac{C_1}{0.5}\sqrt{\frac{L_D}{L}}\left(\frac{H}{\delta}\right) \qquad \text{(D-6)}$$

Where $H$ is the height of the horizontal portion of the cavity/tunnel and $\delta$ is the height of the debris layer on the cavity floor. This shows that a linearly scaled model preserves the ratio of the relative rates for debris removal from the reactor cavity/instrument tunnel region.

# APPENDIX E

## Scoping Calculation For De-Entrainment

A scoping calculation is developed here to establish the amount of debris de-entrained at the 90° turn from the cavity instrument tunnel to the lower containment compartment.

As shown in Figure E-1, the cavity instrument tunnel is assumed to have cross-sectional area $L\ell$ and the opening into the lower containment compartment is assumed to have a cross-sectional area $W\omega$.

The equation of motion for a spherical drop of diameter d and mass m in a gas flow is:

$$m\,\dot{\underline{V}} = mg - C_D\,\frac{4}{3}\,\pi\left(\frac{d}{2}\right)^3 \rho_G \left|\underline{V} - \underline{u}\right| (\underline{V} - \underline{u}) \quad , \tag{E-1}$$

where g is the gravitational constant, $C_D$ is the drag coefficient, $\underline{u}$ is the gas velocity and $\rho_G$ is the gas density.

Equation (E-1) may be re-written as

$$\dot{\underline{V}} = \lambda \left|\underline{V} - \underline{u}\right| (\underline{V} - \underline{u}) + g \tag{E-2}$$

where $\rho_L$ is the density of the drop and

$$\lambda = \frac{3}{4}\left(\frac{1}{d}\right)\frac{\rho_g}{\rho_L}\,C_D. \tag{E-3}$$

For the regime of gas velocities of interest $C_D = 0.44$ and the effects of gravity on the particles may be neglected. The equation of motion then becomes

$$\dot{\underline{V}} = -\lambda \left|\underline{V} - \underline{u}\right| (\underline{V} - \underline{u}). \tag{E-4}$$

Integrating the equation of motion gives

$$\underline{V}(t) = \underline{u}_1 + \frac{(\underline{V}_o - \underline{u}_1)}{1 + \lambda|\underline{V}_o - \underline{u}_1|t} \tag{E-5}$$

where $\underline{V}_o$ is the initial velocity of the particle and $\underline{u}_1$ is the velocity of the gas as it leaves the instrument tunnel.

In terms of the coordinate system displayed in Figure E-2 we have

$$\underline{V}_o = -u\,\hat{\underline{x}} \tag{E-6}$$

while $\underline{u}_1$ is calculated from $\underline{u}$ using the continuity equation

$$\underline{u}_1 = \left(\frac{L\ell}{W\omega}\right) u\,\hat{\underline{y}} \tag{E-7}$$

and for convenience we define

$$\gamma = \left(\frac{L\ell}{W\omega}\right). \tag{E-8}$$

In order to separate the equation of motion into its vector components, we simplify the denominator of Equation (E-5) as

$$\left|\underline{V}_o - \underline{u}_1\right| = \left| -u\hat{\underline{x}} - \gamma u\hat{\underline{y}}\right| = u\sqrt{1 + \gamma^2} \tag{E-9}$$

and for convenience we define

$$\Gamma = \sqrt{1 + \gamma^2}\,. \tag{E-10}$$

Now Equation (E-5) becomes

$$\underline{V}(t) = \underline{u}_1 + \frac{(\underline{V}_o - \underline{u}_1)}{1 + \lambda\Gamma ut} \tag{E-11}$$

Separating Equation (E-11) into its vector components gives

$$V_x(t) = \frac{-u}{1 + \lambda\Gamma ut} \tag{E-12}$$

and,

$$V_y(t) = \gamma u - \frac{\gamma u}{1 + \lambda\Gamma u t} \tag{E-13}$$

Integrating Equations (E-12) and (E-13) gives

$$x(t) = \frac{-1}{\lambda\Gamma} \ln (1 + \lambda\Gamma u t) + x_o \tag{E-14}$$

and

$$y(t) = \gamma u t - \frac{\gamma}{\lambda\Gamma} \ln (1 + \lambda\Gamma u t) + y_o \tag{E-15}$$

For simplicity we assume that the gas velocity in the tunnel changes from $-u\hat{x}$ to $\gamma u\hat{y}$ along the line $y = \frac{L}{W} X$. The initial conditions, $(x_o, y_o)$, are then related as $y_o = \frac{L}{W} x_o$.

For some $(y_o, x_o)$ there will be a time $t_f$ at which $x(t_f) = 0$ and $y(t_f) = L$. Let this $(y_o, x_o)$ be $(y_i, x_i)$. All particles at positions $y_o < y_i$ at time $t_f$ will not make the turn. We define $\alpha = \frac{y_i}{L}$ as the fraction of particles not making the turn.

Equations (E-14) and (E-15) are solved for $\alpha$. Substituting Equation (E-14) into Equation (E-15) yields

$$y(t) = \gamma u t + \gamma(x(t) - x_o) + y_o \tag{E-16}$$

At time, $t_f$, Equation (E-16) becomes

$$L = \gamma u t_f + y_o (1 - \gamma \frac{W}{L}). \tag{E-17}$$

Solving Equation (E-17) for $t_f$ and plugging this expression into Equation (E-16) gives

$$\alpha = \frac{1}{\lambda\Gamma w} \ln \left( 1 + \frac{\lambda\Gamma L}{\gamma} (1 - \alpha (1 - \frac{W}{L} \gamma)) \right) \tag{E-18}$$

This expression can be solved for $\alpha$ iteratively for different cavity dimensions and particle sizes to find the fraction of core material de-entrained at a 90° turn.

## Cavity Instrument Tunnel & Opening Into Lower Containment

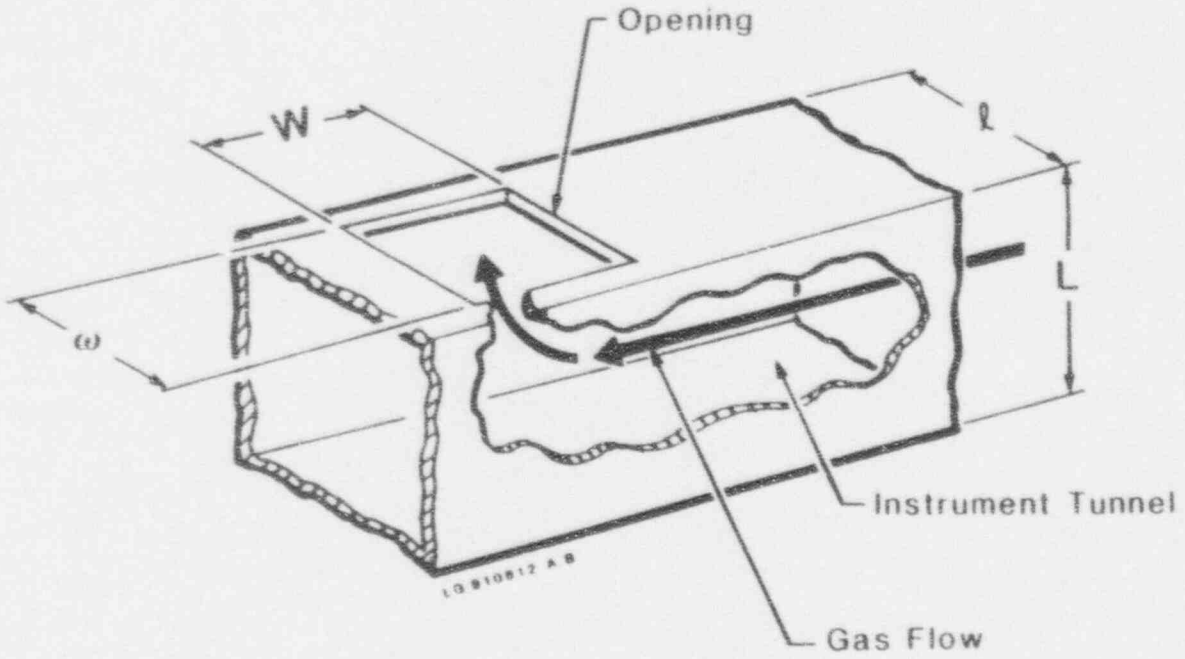


Figure E-1

## Coordinate System in Instrument Tunnel

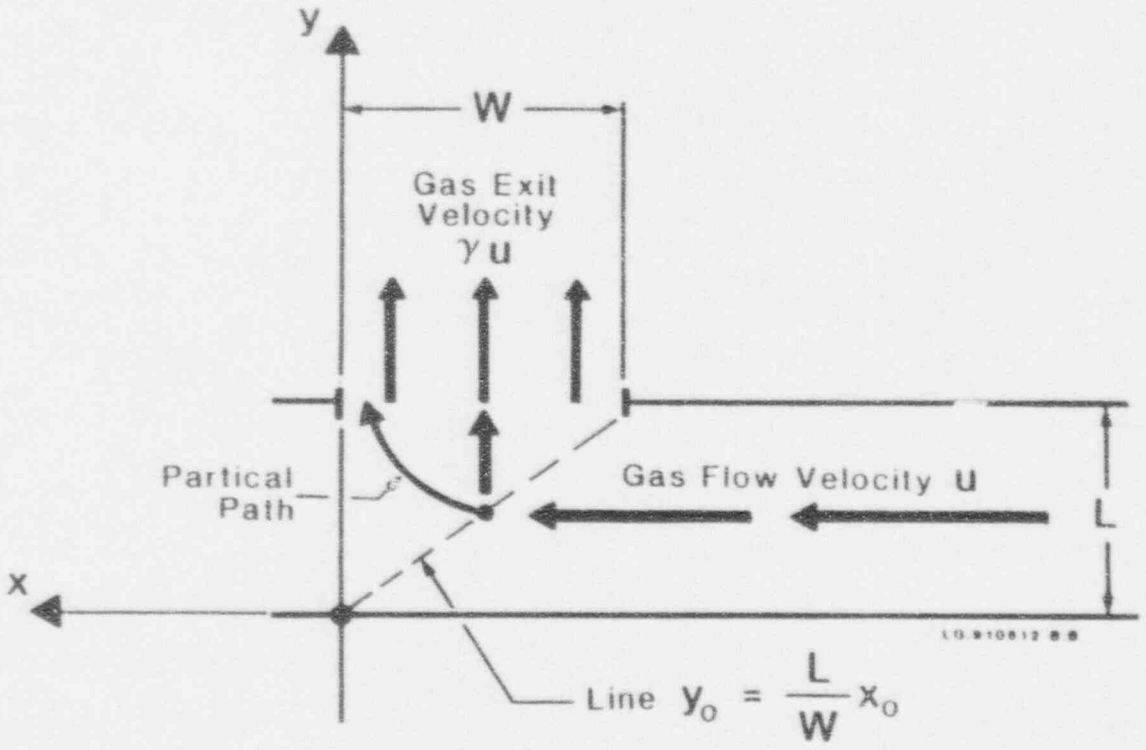


Figure E-2

Tarbell, W. W., et al., 1987b, "Results from the DCH-1 Experiment", SAND86-2483, NUREG/CR-4817, Sandia National Laboratory.

Tarbell, W. W., et al., 1988a, "DCH-2: Results from the Second Experiment Peformed in the Surtsey Direct Heating Test Facility", SAND87-0976, NUREG/CR-4917, Sandia National Laboratory.

Tarbell, W. W., et al., 1988b, "Direct Containment Heating and Aerosol Generation During High-Pressure-Melt Expulsion Experiments", Trans. Am. Nucl. Soc., 57, 361.

Thinnes, G. L., and Moore, R. L., 1989, "Comparison of Thermal and Mechanical Responses of the Three Mile Island Unit 2 Reactor Vessel", Nuclear Technology, Vol. 87, pp. 1036-1049.

Tutu, N. K., et al., 1988, "Debris Dispersed from Reactor Cavities During High-Pressure Melt Ejection Accident Scenarios", NUREG/CR-5146, BNL-NUREG-52147.

Walker, J. V., 1987, "Reactor Safety Research Semi-Annual Report", NUREG/CR-5039, SAND87-2411.

FAUSKE & ASSOCIATES, INC.

CALCULATION NOTE COVER SHEET

SECTION TO BE COMPLETED BY AUTHOR(S):

Page 1

Calc-Note Number FAI/91-56 Revision Number 1

Title PHENOMENOLOGICAL EVALUATION SUMMARY ON MOLTEN CORE-CONCRETE INTERACTION

Project FARLEY NUCLEAR PLANT IPE Shop Order IPE019

Purpose: EVALUATE THE POTENTIAL FOR CONTAINMENT FAILURE DUE TO MOLTEN CORE-CONCRETE INTERACTION (MCCI).

Results Summary: MCCI IS NOT A SIGNIFICANT CONTAINMENT FAILURE MECHANISM (Ref. §4.2 of Attached).

| Author(s): Name (Print or Type) | Signature | Completion Date |
|---|---|---|
| J. P. BURELBACH | James P. Burelbach | 8/92 |
| | | |

SECTION TO BE COMPLETED BY VERIFIER(S):

| Verifier(s): Name (Print or Type) | Signature | Completion Date |
|---|---|---|
| R. D. ASTLEFORD | R D Astleford | 8/10/92 |
| | | |

SECTION TO BE COMPLETED BY MANAGER:

| Responsible Manager: Name (Print or Type) | Signature | Approval Date |
|---|---|---|
| W. E. BERGER | W E Berger | 8/10/92 |
| | | |